

# The Vertical Middepth Ocean Density Profile: An Interplay between Southern Ocean Dynamics and Interior Vertical Diffusivity

XIAOTING YANG<sup>a</sup> AND ELI TZIPERMAN<sup>a,b</sup>

<sup>a</sup> *Department of Earth and Planetary Sciences, Harvard University, Cambridge, Massachusetts*

<sup>b</sup> *School of Engineering and Applied Sciences, Harvard University, Cambridge, Massachusetts*

(Manuscript received 26 August 2021, in final form 30 May 2022)

**ABSTRACT:** The middepth ocean temperature profile was found by Munk in 1966 to agree with an exponential profile and shown to be consistent with a vertical advective–diffusive balance. However, tracer release experiments show that vertical diffusivity in the middepth ocean is an order of magnitude too small to explain the observed 1-km exponential scale. Alternative mechanisms suggested that nearly all middepth water upwells adiabatically in the Southern Ocean (SO). In this picture, SO eddies and wind set SO isopycnal slopes and therefore determine a nonvanishing middepth interior stratification even in the adiabatic limit. The effect of SO eddies on SO isopycnal slopes can be understood via either a marginal criticality condition or a near-vanishing SO residual deep overturning condition in the adiabatic limit. We examine the interplay between SO dynamics and interior mixing in setting the exponential profiles of  $\sigma_2$  and  $\partial_z \sigma_2$ . We use eddy-permitting numerical simulations, in which we artificially change the diapycnal mixing only away from the SO. We find that SO isopycnal slopes change in response to changes in the interior diapycnal mixing even when the wind forcing is constant, consistent with previous studies (that did not address these near-exponential profiles). However, in the limit of small interior mixing, the interior  $\partial_z \sigma_2$  profile is not exponential, suggesting that SO processes alone, in an adiabatic limit, do not lead to the observed near-exponential structures of such profiles. The results suggest that while SO wind and eddies contribute to the nonvanishing middepth interior stratification, the exponential shape of the  $\partial_z \sigma_2$  profiles must also involve interior diapycnal mixing.

**KEYWORDS:** Ocean; Diapycnal mixing; Eddies; Ocean dynamics

## 1. Introduction

A balance between upward advection of cold water and downward diffusion of heat was shown by Munk (1966) to be consistent with the near exponential vertical structure of temperature profile in the middepth Pacific Ocean. In this scenario, some 20 Sv (1 Sv  $\equiv 10^6 \text{ m}^3 \text{ s}^{-1}$ ) of deep water formation at high latitudes returns to the surface via uniform upwelling, balanced by a vertical diffusivity as large as  $10^{-4} \text{ m}^2 \text{ s}^{-1}$ , leading to the observed 1-km exponential depth scale. However, tracer release experiments showed that the actual vertical mixing in the interior middepth ocean is an order of magnitude smaller, while much stronger mixing is observed near the ocean bottom and boundaries (Ledwell et al. 1993; Polzin et al. 1997), due to tidal forcing and breaking of internal waves near topography (Wunsch and Ferrari 2004).

It was therefore suggested by Miller et al. (2020) that a Munk-like balance in strong-mixing boundary regions, with a large vertical velocity and large diapycnal mixing there, can lead to the observed 1-km scale of the middepth (1–3 km) temperature profiles, which is then communicated to the interior via horizontal eddy mixing, as was also suggested by Munk and Wunsch (1998). While the Munk idea was based

on assuming that the vertical mixing coefficient and upwelling are constant in the vertical, Tziperman (1986) showed, and Miller et al. (2020) verified, that the near-exponential potential density profile is, in fact, not sensitive to modest vertical variations in these two variables.

This observed boundary enhancement of vertical mixing also inspired studies of such mixing on the overturning circulation (Samelson 1998; Scott and Marotzke 2002). These studies showed that upwelling is concentrated where vertical mixing is enhanced, instead of being uniform over the global ocean. In related research, Ferrari et al. (2016) found that sloping boundaries and enhanced bottom mixing lead to enhanced upwelling near the boundaries and possibly to downwelling in the interior. Mashayek et al. (2015) found that the stratification vertical length scale varied only by about a factor of 2 in the middepth range above the abyssal layer where vertical mixing is bottom-intensified, implying that the middepth stratification profile is approximately exponential with a length scale of about 1 km.

An alternative approach that has been suggested for explaining the existence of a nonvanishing middepth stratification relies on Southern Ocean (SO) eddies rather than on vertical mixing. The Southern Ocean is dynamically special in that it is unblocked by meridional continental boundaries above the sill depth. Therefore, no geostrophic meridional flows are allowed above the sill because no zonal pressure gradient can be sustained without solid meridional boundaries. This means the northward Ekman transport induced by the westerlies above the Southern Ocean can only be returned southward below the sill depth, geostrophically, or in the

Supplemental information related to this paper is available at the Journals Online website: <https://doi.org/10.1175/JPO-D-21-0188.s1>.

Corresponding author: Xiaoting Yang, [xiaoting\\_yang@g.harvard.edu](mailto:xiaoting_yang@g.harvard.edu)

bottom boundary layer. This wind-induced overturning is expected to meridionally steepen the isopycnal surfaces in the SO. The baroclinic instability associated with these sloping isopycnals generates eddies that act to flatten the isopycnals. The competition between the wind forcing and eddies in the Southern Ocean, therefore, results in sloping isopycnals. These sloping isopycnals map the surface density distribution in the SO to a vertical distribution at the northern boundary of the SO, which is the southern boundary of the interior (by “interior” we mean north of the SO and away from far north convection sites), setting the interior middepth stratification that way (Vallis 2000; Wolfe and Cessi 2010; Nikurashin and Vallis 2011). In the Munk picture, the middepth stratification vanishes in the limit of vanishing vertical mixing. When these SO eddy dynamics are taken into account, the middepth stratification does not vanish even if the overturning circulation is adiabatic and the interior diabatic diffusivity is neglected. In this adiabatic limit, the MOC return flow to the surface occurs along sloping isopycnals in the SO (Vallis 2000; Wolfe and Cessi 2010; Nikurashin and Vallis 2011). However, it has been pointed out by Miller et al. (2020) that the middepth profile of potential density in numerical simulations performed at this limit is not exponential. Nikurashin and Vallis (2011) pointed out that in the presence of large vertical diffusion, the stratification is determined by the Munk balance rather than by the SO wind and eddies. They do not discuss the issue of exponential stratification, and also suggest that this regime may be relevant to the abyssal stratification rather than the middepth one.

The idea that eddies strongly influence isopycnal slopes is of critical importance for the above studies showing how eddies can lead to a nonvanishing middepth interior stratification in the adiabatic overturning picture, and two mechanisms were proposed to explain the relation between eddies and isopycnal slopes more generally. One involves the idea of marginal criticality, also referred to as eddy saturation, and the other of a fully compensated SO deep residual circulation, and both are discussed below. In the adiabatic limit in which the SO eddies are strong and the interior diapycnal mixing is weak, both of these mechanisms lead to isopycnal slopes in the SO that depend only on the SO winds and eddy dynamics. This means that the middepth ocean stratification north of the SO is then fully determined by the SO wind, eddies, and SO surface buoyancy distribution in the limit of weak interior vertical mixing (Jansen and Ferrari 2012). These idealized limits are useful extreme states which we examine in this paper to identify their relation to the observed interior near-exponential middepth profiles of  $\sigma$  and  $\partial_z \sigma$ .

The first idea is that slopes are at the so-called marginal criticality (Stone 1978; Jansen and Ferrari 2012, 2013a,b). At marginal criticality, larger slopes, which can be a result of changes in external forcing, would lead to eddy formation via baroclinic instability, drawing available potential energy (APE) from the mean slopes, and therefore flattening them back to the original state of marginal criticality. This is equivalent to saying that the mean state of the system does not respond to changes in the exterior forcing, such as surface wind stress. This marginal criticality may be diagnosed via the ratio

between the Rhines scale and the deformation radius (Jansen and Ferrari 2012), or via the ratio between the potential vorticity gradient due to layer thickness variations and the  $\beta$  effect (Jansen and Ferrari 2013a). If eddies are sufficiently efficient in drawing APE from the mean slopes and thus maintain a state whose criticality is approximately one, isopycnal slopes are independent of changes in the external forcing, such as wind and interior diapycnal mixing. However, it has been suggested that ocean eddies are not expected to be sufficiently effective in this sense, and slopes are therefore not necessarily at marginal criticality (Jansen and Ferrari 2012). An equivalent view of this marginal criticality idea is that of eddy saturation: as SO winds get stronger the isopycnal slopes stop responding at some point due to the effect of ocean eddies that keep the slopes at saturation (Munday et al. 2013).

The second way to view the role of eddies in affecting SO isopycnal slopes is that eddies set these slopes via buoyancy advection that is opposite and nearly equal to the mean advection driven by the wind-driven overturning. This implies that the SO residual circulation (nearly) vanishes, and it was shown that isopycnal slopes are then determined by a balance between SO wind forcing and eddies (Gnanadesikan 1999; Marshall and Radko 2003; Wolfe and Cessi 2010; Nikurashin and Vallis 2011). It has also been shown that the SO deep residual circulation is expected to vanish in the limit of zero interior diffusivity and in the absence of surface buoyancy forcing in the SO (Marshall and Radko 2003). In this limit, SO eddies and winds would be setting the SO isopycnal slopes and therefore the interior middepth ocean stratification without contribution by other physical processes away from the SO. Wolfe and Cessi (2011) showed in eddy-resolving numerical simulations that as the interior diffusivity vanishes, the deep residual circulation in the SO indeed nearly vanishes. On the other hand, the residual overturning and eddy activity in the SO (and therefore the equivalent GM coefficient; Gent and McWilliams 1990) have been found to be sensitive to changes in vertical mixing in idealized GCM simulations (Munday et al. 2013).

We can summarize the role of the SO residual circulation identified in previous studies as follows. Wolfe and Cessi (2010) found that the dynamics of the SO are nearly adiabatic beneath the surface layer, and that a middepth interior ocean stratification can exist even with a vanishing interior vertical diffusivity. Similarly, Nikurashin and Vallis (2011) found that for weak diapycnal interior mixing typical of the middepth ocean, the middepth overturning circulation and stratification are primarily controlled by the wind and eddies in the SO channel, with diapycnal mixing playing a minor role. In the limit of weak diapycnal interior mixing, the interior stratification, therefore, does not vanish and is determined by the SO winds and eddies (as represented by the GM coefficient).

In this paper, we accept the above premise that the SO wind and eddies allow for a nonvanishing middepth stratification in the limit of weak interior diapycnal mixing. We show using the WOCE dataset (Gouretski and Koltermann 2004) that the observed interior middepth  $\sigma_2$  profiles agree well with their exponential fits. For an actually exponential profile, the scale of the exponential could be estimated as  $\sigma_{2,z}/\sigma_{2,zz}$

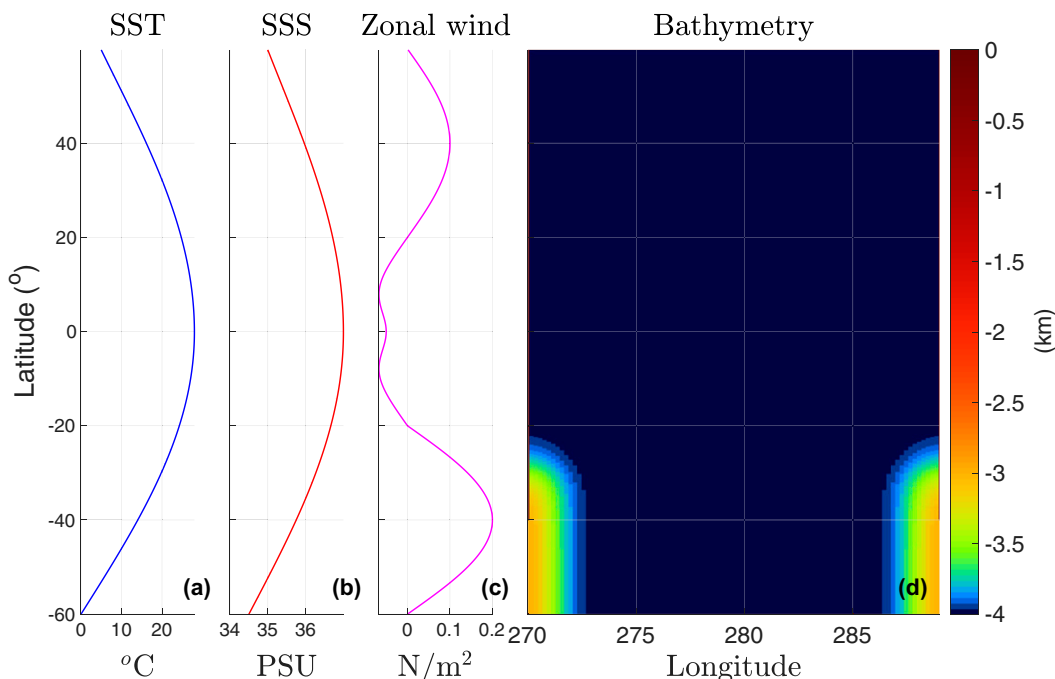


FIG. 1. The model configuration. (a) SST restoring profile; (b) SSS restoring profile; (c) zonal wind stress; (d) colors: bathymetry (km).

(Mashayek et al. 2015). We also show that the agreement between vertical derivatives of  $\sigma_2$  and corresponding exponential fits deteriorates with higher orders of derivatives used, and that the fits then tend to have different vertical length scales. This is consistent with the view we adopt here that the observed stratification is “near-exponential” rather than exactly so. We then show, though, that for this potential density profile to be near-exponential, as robustly observed (Munk 1966; Miller et al. 2020), diapycnal ocean mixing is necessary and should not be ignored. Throughout this paper, the term “exponential” or “near-exponential” refers to a good agreement of the profile of potential density or its vertical derivative to an exponential fit.

We use numerical eddy-permitting simulations to show that the Southern Ocean isopycnal slopes and thus the near-exponential interior profiles of  $\sigma_2$  and  $\partial_z \sigma_2$  are influenced by the interior vertical diffusivity. The SO wind and eddies cannot determine the near-exponential interior  $\partial_z \sigma_2$  profile independently of processes in the ocean interior north of the SO. For this purpose, we change values of the diapycnal diffusivity  $\kappa_v$ , only north of the SO channel, in a range of small to unrealistically large values, to study the possible response of the SO isopycnal slopes to changes in the interior basin diapycnal mixing (section 3b). We find that both isopycnal slopes and eddy activity in the SO, as reflected in measures of both the marginal criticality and residual circulation there, respond to changes in the interior mixing. Miller et al. (2020) used coarse-resolution simulations and focused on the equivalence between the boundary-intensified vertical mixing and a uniform strong vertical mixing in making the middepth ocean profile of potential density and its vertical

derivative nearly exponential. On the other hand, the present work uses eddy-permitting simulations to directly evaluate the response of SO eddies to changes in interior vertical mixing. Furthermore, we do not consider a “realistic” boundary-intensified spatial distribution of vertical mixing but focus on the interaction of SO dynamics, interior vertical mixing and middepth stratification.

This paper is organized as follows. We describe the experimental designs in section 2. Results are presented in section 3 which is further divided into a discussion of the middepth profiles of  $\sigma_2$  and  $\partial_z \sigma_2$  (section 3a), and the response of the Southern Ocean to changes in interior vertical mixing (section 3b). We discuss marginal criticality and residual circulation in section 4, and we conclude in section 5. The term “stratification” in this paper refers to the vertical distribution of density in the ocean, as quantified by either  $\sigma_2$  or  $\partial_z \sigma_2$  profiles. The square of the Brunt–Väisälä frequency will be referred to as  $N^2$ .

## 2. Model configuration

We use an idealized configuration of the Massachusetts Institute of Technology General Circulation model (MITgcm; Marshall et al. 1997). The idealized geometry and bathymetry of our simulations shown in Fig. 1d are motivated by the course-resolution simulations used by Nikurashin and Vallis (2011, 2012) and Miller et al. (2020), and the eddy-permitting configurations used by Wolfe and Cessi (2010, 2011).

This domain ranges from 60°S to 60°N, with a re-entrant channel between 60° and 40°S. In the channel, there is a smoothed sill at a depth of 3 km. This sill guarantees that the

TABLE 1. Numerical parameters.

$A_h$	$A_4$	$A_r$	$\kappa_4$	$r_b$
$10 \text{ m}^2 \text{ s}^{-1}$	$1.5 \times 10^{10} \text{ m}^4 \text{ s}^{-1}$	$10^{-4} \text{ m}^2 \text{ s}^{-2}$	$1.5 \times 10^{10} \text{ m}^4 \text{ s}^{-1}$	$2 \times 10^{-4} \text{ s}^{-1}$

transport of the circumpolar current is within a realistic range ( $\sim 100$  Sv), and it is smoothed to avoid spurious numerical noise in the vertical velocity that may influence stratification, which is the focus of this paper. Otherwise, the bathymetry is flat at a depth of 4.2 km. The horizontal resolution is  $0.2^\circ \times 0.2^\circ$ , and we use 51 vertical layers in total, whose thicknesses range from 5 m near the surface to 125 m near the bottom. Although it would be interesting to investigate the exponential profile issue using a realistic World Ocean configuration, we use the above idealized geometry to be able to compare and contrast our results to those of the above cited papers which dealt with the middepth stratification. We use a narrow basin that is only  $20^\circ$  wide to limit the computational cost, due to the relatively high horizontal resolution used here.

The model is forced at the surface by restoring to longitude-independent temperature and salinity fields using a restoring time scale of 10 days, and with a zonal wind stress profile (Figs. 1a–c). Having both temperature and salinity allows us to use a realistic equation of state. Yet, because we choose the surface temperature and salinity profiles and their restoring times to be identical for simplicity, the two components do not represent independent degrees of freedom as in the real ocean, and their interior distributions are very similar. The model parameters that are identical for all cases include a horizontal harmonic viscosity ( $A_h = 10 \text{ m}^2 \text{ s}^{-1}$ ), horizontal biharmonic viscosity ( $A_4 = 1.5 \times 10^{10} \text{ m}^4 \text{ s}^{-1}$ ), vertical viscosity ( $A_v = 10^{-4} \text{ m}^2 \text{ s}^{-1}$ ), horizontal biharmonic diffusivity ( $\kappa_4 = 1.5 \times 10^{10} \text{ m}^4 \text{ s}^{-1}$ ), and a linear bottom drag coefficient ( $r_b = 2 \times 10^{-4} \text{ s}^{-1}$ ). These parameters are summarized in Table 1. We use a nonlinear equation of state, following Jackett and McDougall (1995). Considering the high-resolution used here, mesoscale eddies are at least partially resolved (a snapshot is shown in Fig. S1 in the online supplemental material), and the Gent and McWilliams (1990) scheme is therefore not used. The grid spacing is approximately 14 km in the channel (at  $50^\circ\text{S}$ ) and is comparable to the simulated (and observed) deformation radius there, implying that our resolution is only marginal for resolving eddies in the SO. Diapycnal mixing and convection are represented using the  $K$ -profile parameterization scheme (Large et al. 1994), and we use the third-order direct space time (DST) flux limiter for advection (33 in MITgcm).

We focus on the effect of vertical mixing in the domain away from the SO, north of  $40^\circ\text{S}$ , on the middepth stratification and SO eddies. Therefore, the vertical diffusivity parameter in the Southern Ocean itself is unchanged from its control value ( $10^{-5} \text{ m}^2 \text{ s}^{-1}$ ) for all cases. We use a series of values for this vertical diffusivity north of the channel:  $10^{-5}$ ,  $10^{-4}$ ,  $2 \times 10^{-4}$ ,  $4 \times 10^{-4}$ ,  $6 \times 10^{-4}$ ,  $8 \times 10^{-4}$ , and  $10^{-3} \text{ m}^2 \text{ s}^{-1}$ . The value of  $\kappa_v$  varies linearly between the SO channel and the interior over a  $5^\circ$  wide latitudinal range north of  $40^\circ\text{S}$  (Table 2). The vertical diffusivity north of the channel is uniform instead

of having the boundary-intensified distribution as used by Miller et al. (2020). This uniform value is meant to represent the global effect of vertical mixing processes in the ocean that are observed to be enhanced near the ocean bottom and rough topography. The choice to only change vertical diffusivity north of the channel is artificial, of course, because  $\kappa_v$  is affected by the strength of the interactions of tidal forcing and internal waves with topography in the ocean (Wunsch and Ferrari 2004) and is not expected to necessarily be small in the SO itself. We also explore a range of  $\kappa_v$  that is unrealistically large. In both cases, these design choices are due to our desire to identify the effects of diapycnal mixing north of the SO on stratification and eddies within the SO. Munday et al. (2011) has used similar model configurations to study how changes in  $\kappa_v$  away from the SO can influence the Antarctic Circumpolar Current (ACC) transport via a global adjustment of pycnocline depths.

We run the simulations until a statistical steady state is reached (time series of layerwise-averaged temperature and salinity converge) and then run the model for 20 more years. The temporally averaged model variables ( $T$ ,  $S$ , velocities) are calculated using model output from these last 20 years. Nonlinear terms in the  $\sigma_2$  budget and the eddy kinetic energy budget are averaged using bidaily data over the last 10 years.

### 3. Results

This section is divided into two parts: the response of mid-depth stratification to changes in interior vertical diffusivity is discussed in section 3a and the response of Southern Ocean eddies in section 3b. In section 3a we show that the quality of exponential fits to the vertical profiles of potential density and their vertical derivative improves with an increasing interior vertical diffusivity  $\kappa_v$ . At the same time, isopycnal slopes in the SO increase and SO eddy activity strengthens as the interior  $\kappa_v$  increases. We explain that this suggests that SO eddies are not able to maintain the SO isopycnal slopes at marginal criticality, which we later use to discuss the processes responsible for the middepth interior ocean stratification. We then explain the eddy response by analyzing the Eady growth rate and the eddy kinetic energy in the Southern Ocean (section 3b).

TABLE 2. Summary of the numerical simulations.

Case No.	Code name	Interior $\kappa_v$
1	Control	$10^{-5}$
2	$\kappa_v \times 10$	$10^{-4}$
3	$\kappa_v \times 20$	$2 \times 10^{-4}$
4	$\kappa_v \times 40$	$4 \times 10^{-4}$
5	$\kappa_v \times 60$	$6 \times 10^{-4}$
6	$\kappa_v \times 80$	$8 \times 10^{-4}$
7	$\kappa_v \times 100$	$10^{-3}$

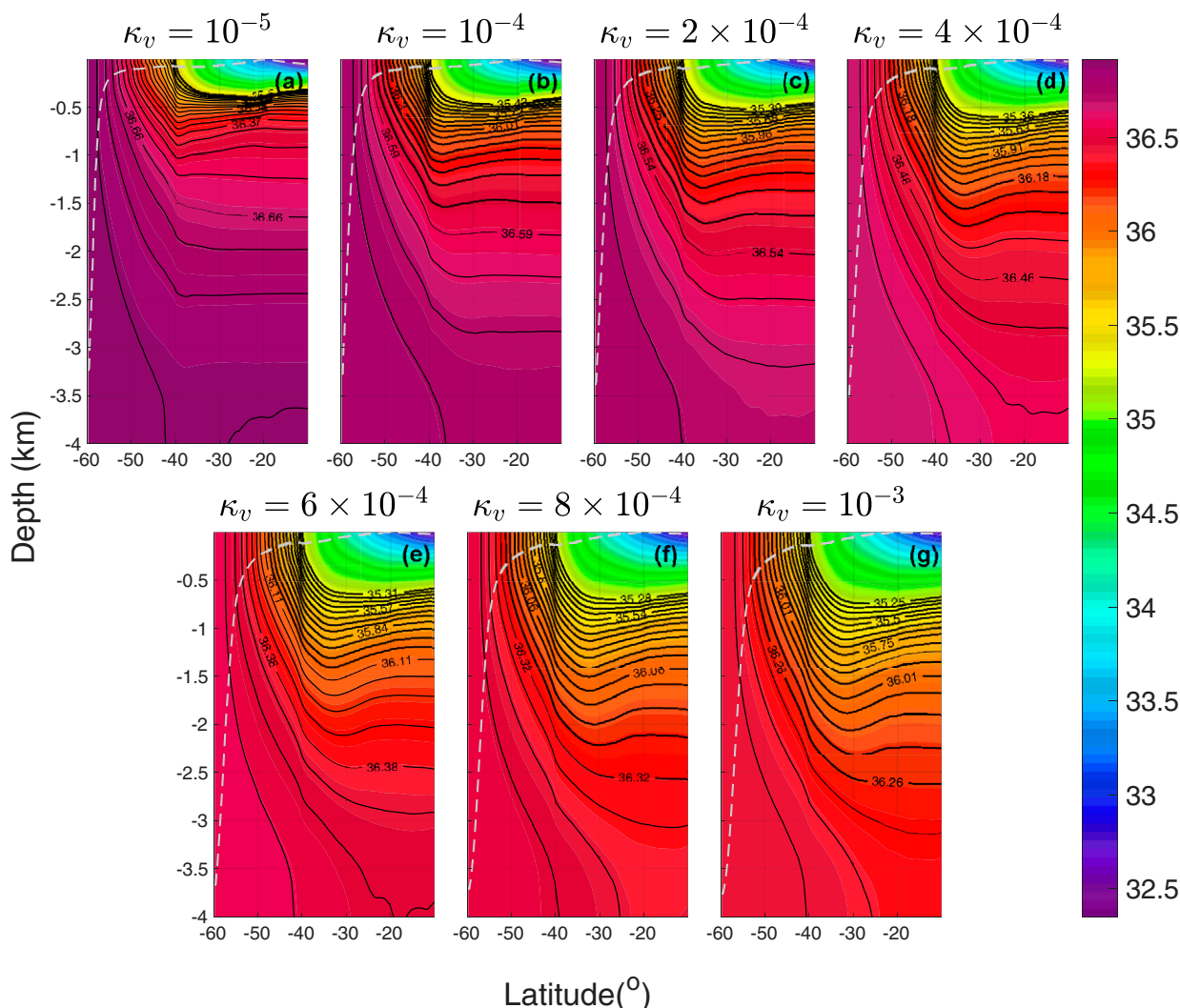


FIG. 2. Colors: zonally averaged  $\sigma_2$  south of  $15^\circ\text{S}$ . Black contours: 20 isopycnal surfaces that originate from the surface of the southern channel. Gray dashed line: bottom of the surface mixed layer, calculated by the  $K$ -profile parameterization package. (a) Control case with vertical diffusivity denoted  $\kappa_v$ , (b)  $\kappa_v \times 10$ , (c)  $\kappa_v \times 20$ , (d)  $\kappa_v \times 40$ , (e)  $\kappa_v \times 60$ , (f)  $\kappa_v \times 80$ , and (g)  $\kappa_v \times 100$ .

*a. Middepth stratification*

As the vertical diffusivity in the interior is increased, the middepth ocean gets warmer and therefore lighter as more heat diffuses downward (Figs 2 and Fig. S2). In Fig. 2, 20 isopycnals that both outcrop in the SO channel and exist at mid-depth at  $40^\circ\text{S}$  are plotted (solid black lines). It is clear that the slopes of these isopycnal surfaces in the SO become steeper as the interior  $\kappa_v$  is increased. With stronger downward heat diffusion, the interior warms and isopycnals corresponding to larger density move downward (Munday et al. 2011). For SO isopycnals to be able to link the interior density distribution to the prescribed surface density distribution at the surface of the channel, these SO isopycnals must be steeper in the higher interior diffusivity runs. At the same time, the SO surface also becomes lighter (Fig. 3c). This will partly counteract the steepening effect discussed above. The net effect of these

two mechanisms is steeper isopycnal surfaces in the southern channel (Figs. 3a,b). Figures 2 and 3a clearly show that the slopes of the isopycnal surfaces that connect the surface of the southern channel and the southern boundary of the interior basin between 1- and 3.5-km depth are systematically steeper as the interior  $\kappa_v$  is increased. However, the slopes of the densest isopycnal surfaces are comparable in these simulations, because these SO isopycnals which reach the ocean bottom at the northern end of the ACC outcrop near the southern boundary of the model domain, scaling these slopes to be approximately  $-H/l$  ( $l$  is the width of the channel and  $H$  is the depth of SO). The steepening of the isopycnals in response to changes in interior vertical mixing has also been found by Baker et al. (2021). In their work, they used a double-basin coarse-resolution configuration and increased vertical mixing only in the wide basin (Pacific-like). In our work, on the other hand, the diffusive upwelling occurs in the basin where

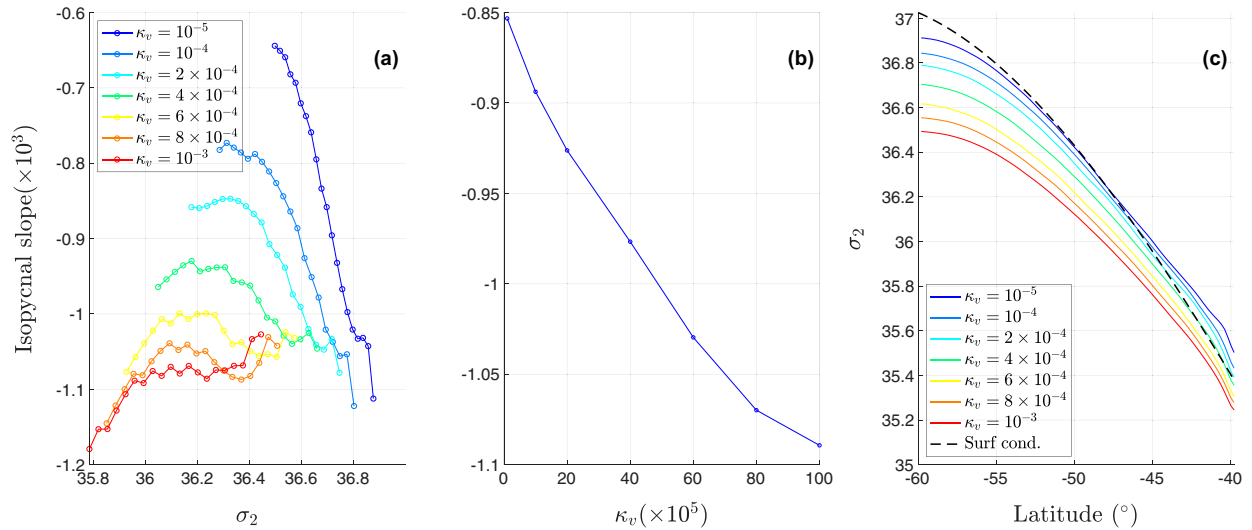


FIG. 3. (a),(b) The averaged isopycnal slopes, calculated using the 20 isopycnal surfaces that outcrop in the SO channel and exist between 1- and 3.5-km depth at 40°S (in other words, relevant to interior middepth ocean stratification). (a) Averaged slopes for the 20 isopycnal surfaces in the channel, as functions of latitude, in all cases (color). (b) Averaged isopycnal slope of the same 20 isopycnal surfaces at all latitudes in the channel, for each case, as a function of interior  $\kappa_v$ . (c) Zonally averaged  $\sigma_2$  at the surface in the channel for all cases (colored lines) and the surface restoring boundary condition (dashed black line).

deep water formation happens as well due to our choice of a single basin configuration.

The criticality parameter can be defined as  $\xi \equiv fs/\beta H$ , where  $f = 2\Omega \sin\theta$  is the Coriolis parameter,  $\beta$  is the meridional gradient of  $f$ ,  $s$  is the isentropic or isopycnal slope, and  $H$  is the depth of the isopycnal layer in the ocean. In the atmosphere, the isentropes that intersect with the surface in the tropics reach the top of the troposphere near the poles, implying a state of marginal criticality ( $\xi \approx 1$ ; Jansen and Ferrari 2013a). Such a conclusion cannot be drawn for the Southern Ocean in our simulations: the response of the isopycnal slopes in the Southern Ocean to interior  $\kappa_v$  changes implies that SO eddies are not sufficiently efficient to maintain a state of marginal criticality, consistent with Jansen and Ferrari (2012). In fact, we find that the SO in our simulations is in a supercritical state and criticality increases as interior  $\kappa_v$  increases (appendix B, Fig. S3).

The averaged interior vertical profiles shown in this section are calculated between 30°S and 30°N, and in regions that are at least three degrees away from the western and eastern boundaries. Figure 4 shows the averaged interior vertical profiles of  $\sigma_2$  output by the model (solid blue lines) and the corresponding exponential fit (dashed red lines) calculated between 1 and 3.5 km depth. The errors in the exponential fit of the profiles of  $\sigma_2$  are small even in the limit of small interior  $\kappa_v$  (control case). At the same time, the exponential decay scale ( $L_{\text{exp}}$ ) decreases for stronger vertical mixing, consistent with Munk (1966). It is also noted that  $L_{\text{exp}}$  is in a range that agrees with the observed 1 km scale in simulations where  $\kappa_v$  is large,  $10^{-4}$  or  $2 \times 10^{-4} \text{ m}^2 \text{ s}^{-1}$ .

However, the quality of the exponential fit to the profiles of  $\partial_z \sigma_2$  is poor at low vertical mixing values and improves considerably for stronger vertical mixing values (Fig. 5). The

fitted profile of  $\partial_z \sigma_2$  is almost a constant in depth [having an exponential depth scale of  $\mathcal{O}(10^4)$  km for a fit between 1- and 3.5-km depth range] in the control simulation. The  $\partial_z \sigma_2$  profile itself indeed does not show an exponential shape in this case but rather is wiggly. To quantify how well the exponential fits agree with the model output, we define the relative error between these two profiles as

$$r = \sqrt{\frac{\sum_k [\partial_z \tilde{\sigma}_2(k) - \partial_z \tilde{\sigma}_{2,\text{exp}}(k)]^2 dZ(k)}{\sum_k \partial_z \tilde{\sigma}_2^2 dZ(k)}}, \quad (1)$$

in which  $k$  is the vertical model level index,  $\partial_z \sigma_2$  is calculated from the model output,  $\partial_z \sigma_{2,\text{exp}}$  is that from the exponential fit, and  $dZ(k)$  is the thickness of the  $k$ th model layer. The symbol  $(\tilde{\cdot})$  refers to the vertical profile with the vertical mean (weighted by layer thickness) removed [e.g.,  $\tilde{\sigma}_2 \equiv \sigma_2 - \sigma_{2,\text{avg}}$ , where  $\sigma_{2,\text{avg}} = \sum_k \sigma_2(k) dZ(k) / \sum_k dZ(k)$ ]. The  $r$  values are given in Fig. 5. We observe a steady improvement of the agreement between the model output profile and the exponential fit, as interior  $\kappa_v$  is increased. The significant deviation of the  $\partial_z \sigma_2$  profile from the exponential fit in the control (low diffusivity) case may be explained by the middepth thermostat at about 1-km depth due to the deep-water formation in the northern high-latitude regions (Fig. S2a). As interior vertical diffusivity is enhanced, this thermostat is eroded, giving rise to an interior profile closer to an exponential shape. The narrowness of the basin results in relatively weak overturning circulation (Fig. S5) and therefore a small zonal isopycnal surface tilting. This means that horizontal averages in our simulation involve similar density ranges at different horizontal positions. This makes the thermostat more prominent in the

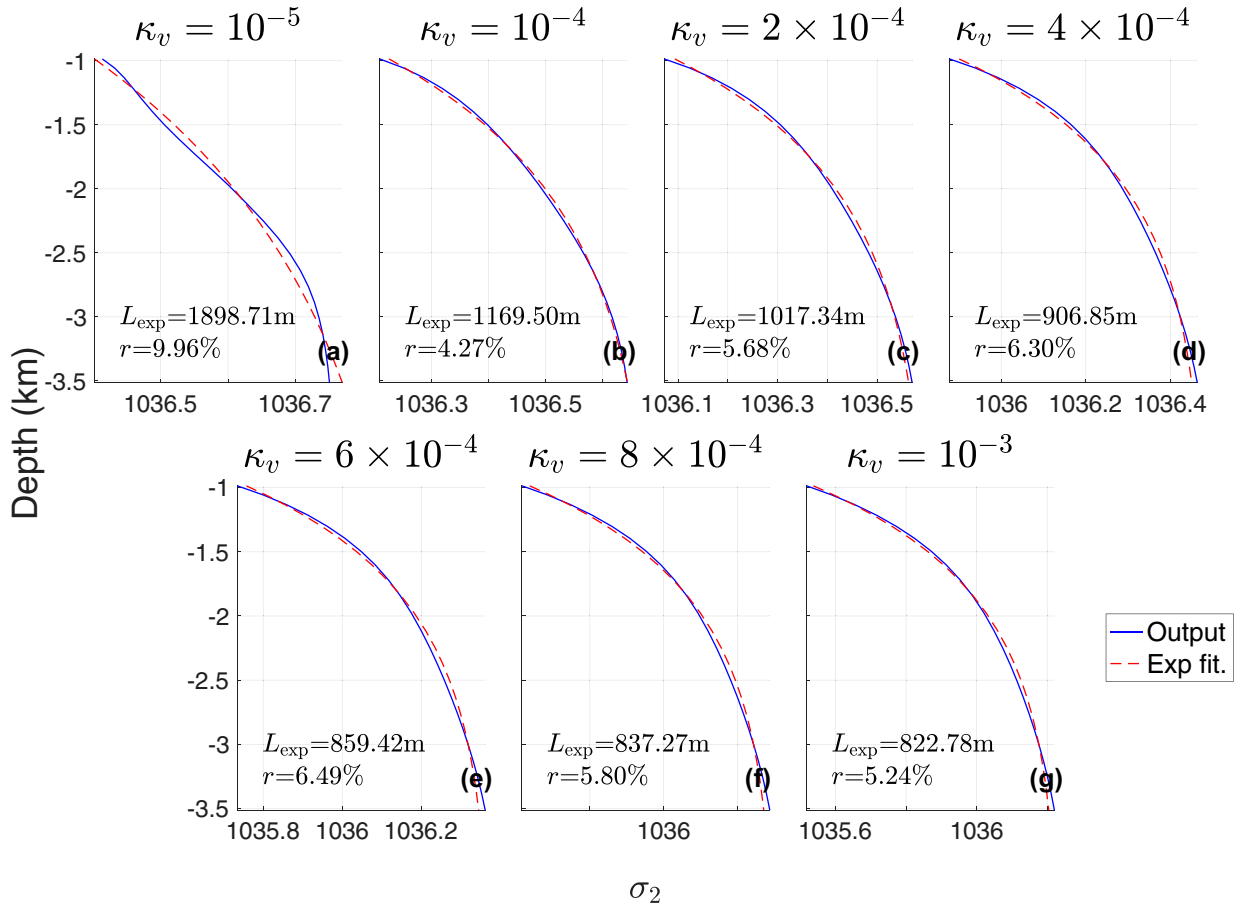


FIG. 4. Exponential fit of the vertical profiles of  $\sigma_2$  averaged between  $30^\circ\text{S}$  and  $30^\circ\text{N}$ ,  $3^\circ$  from the western and the eastern boundaries. The fit coefficients are calculated between 1- and 3.5-km depth. Red dashed line: exponential fit;  $L_{\text{exp}}$ : exponential decay depth scale. (a) Control case, (b)  $\kappa_v \times 10$ , (c)  $\kappa_v \times 20$ , (d)  $\kappa_v \times 40$ , (e)  $\kappa_v \times 60$ , (f)  $\kappa_v \times 80$ , and (g)  $\kappa_v \times 100$ .

horizontal averages and therefore the vertical profile in the low diffusion case farther from an exponential.

We find that the vertical scale of the interior averaged profiles of  $\sigma_2$  compares better with the 1-km scale derived from observed temperature profiles in Munk (1966) than  $\partial_z \sigma_2$  profiles, for all  $\kappa_v$  values. In this paper, we are comparing vertical profiles of  $\sigma_2$  and  $\partial_z \sigma_2$  instead of temperature, considering the nonlinear equation of state. In observations, the vertical scales of  $\partial_z \sigma_2$  profiles are also systematically smaller than the 1-km scale (Fig. S8), consistent with our simulations.

The agreement between  $\sigma_2$  or  $\partial_z \sigma_2$  profiles and exponential fits in simulations using enhanced interior vertical diffusivity is consistent with the quality of exponential fits to observed profiles (Figs. S7 and S8). We also show in the supplemental material that the fitted length scales of the  $\sigma_2$  and the  $\partial_z \sigma_2$  profiles are not necessarily identical, implying that such profiles are only *nearly* exponential.

Munk (1966) assumed a temperature budget between upward mean flow advection and downward diffusion with  $\kappa_v \sim 10^{-4} \text{ m}^2 \text{ s}^{-1}$ , while Wolfe and Cessi (2010) found that horizontal eddy transport played a dominant role in this budget in the limit of small vertical diffusivity. The  $\sigma_2$  budget is

calculated here based on the temperature and salinity budgets at steady state,

$$\mathbf{u}_H \cdot \nabla_H \bar{C} + \bar{w} \partial_z \bar{C} + \overline{\mathbf{v}' \cdot \nabla \mathbf{C}'} = -\kappa_4 \nabla^4 C + \text{Vert diff.} \quad (2)$$

In this equation,  $C$  is the temperature or salinity,  $\bar{(\cdot)}$  stands for a time average, and  $(\cdot)'$  is a deviation from the time average. The symbol  $\mathbf{u}_H$  denotes the horizontal velocity vector,  $\mathbf{v}$  is the 3D flow field vector, and  $w$  is the vertical velocity. The terms  $\nabla_H$  and  $\nabla$  are the horizontal and 3D gradient operators, respectively. Last,  $-\kappa_4 \nabla^4 C$  and “Vert diff” terms are model horizontal and vertical diffusion terms due to parameterized eddy diffusion in the horizontal direction (biharmonic) and parameterized small-scale turbulent mixing in the vertical direction. The corresponding terms in the  $\sigma_2$  budget are calculated based on the temperature and salinity budget following the chain rule applied to the nonlinear equation of state (e.g., the zonal advection term  $u \partial_z \sigma_2 \equiv \partial_T \sigma_2 u \partial_x T + \partial_S \sigma_2 u \partial_x S$ ). We use this chain rule instead of directly evaluating the terms in the  $\sigma_2$  budget, because temperature and salinity are conserved by the model and therefore their budgets are closed. The vertical profiles of each term in the  $\sigma_2$  budget are shown in Fig. 6.

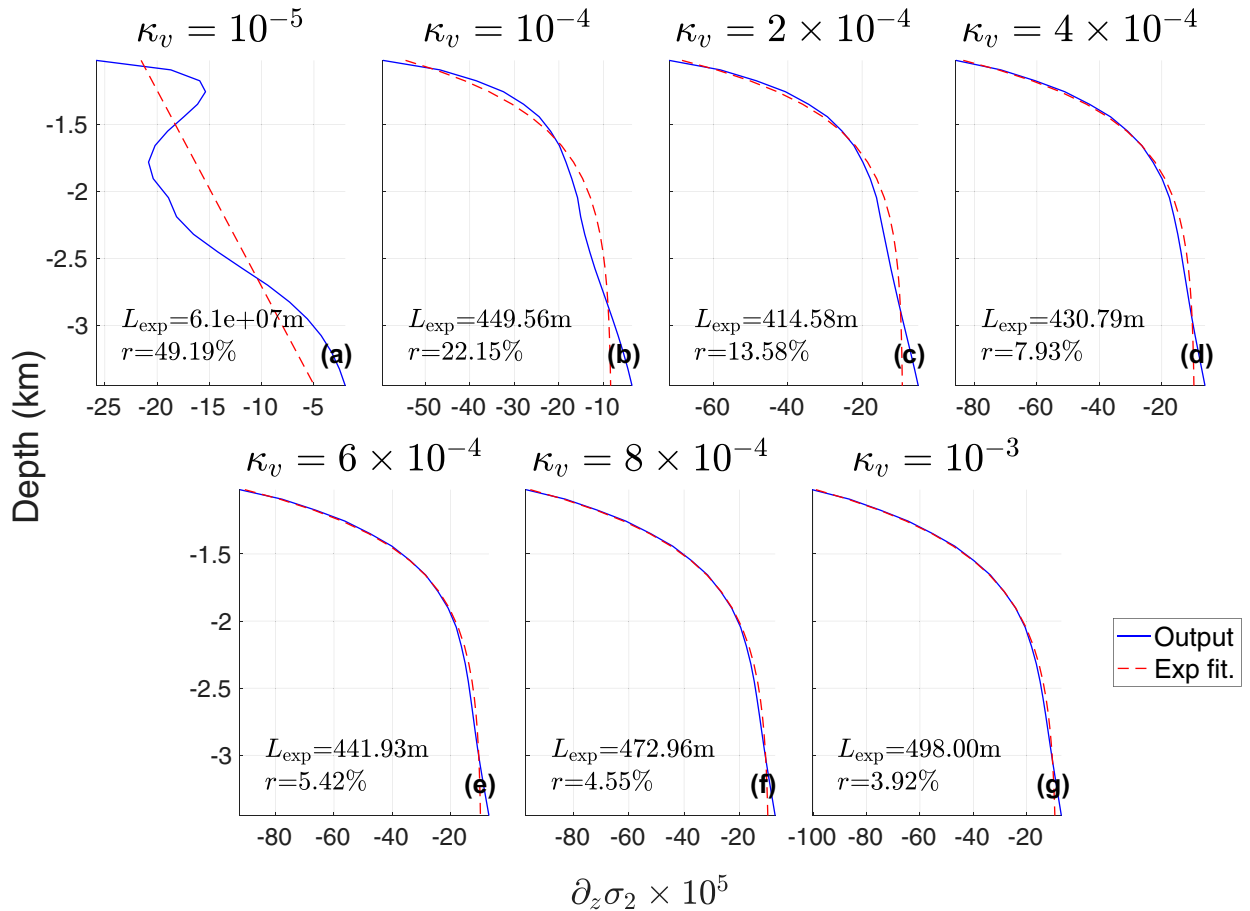


FIG. 5. Exponential fit of the vertical profiles of  $\partial_z \sigma_2$  averaged between 30°S and 30°N, 3° from the western and the eastern boundaries. The fit coefficients are calculated between 1- and 3.5-km depth. Blue solid line: model output, red dashed line: exponential fit;  $L_{\text{exp}}$ : exponential decay depth scale;  $r$ : the relative error between the model output and exponential fit,  $r = \sqrt{\sum [\partial_z \bar{\sigma}_2(k) - \partial_z \bar{\sigma}_{2,\text{exp}}(k)]^2 dZ(k)} / \sqrt{\sum \partial_z \bar{\sigma}_2(k)^2 dZ(k)}$ . (a) Control case, (b)  $\kappa_v \times 10$ , (c)  $\kappa_v \times 20$ , (d)  $\kappa_v \times 40$ , (e)  $\kappa_v \times 60$ , (f)  $\kappa_v \times 80$ , and (g)  $\kappa_v \times 100$ .

In the limit of small interior diffusivity (Fig. 6a, control case), the dominant balance in the  $\sigma_2$  budget is between vertical mean flow advection (red line) and eddy advection (cyan line), in which the horizontal components are dominant (not shown). The vertical diffusion term (dashed green line) only plays a minor role with sign changes in the vertical direction. This dominant balance is consistent with Wolfe and Cessi (2010). When the interior  $\kappa_v$  is larger, the dominant balance becomes between vertical mean flow advection and explicit vertical diffusion, again consistent with Munk (1966). However, the two terms never perfectly balance each other even in the  $\kappa_v \times 100$  case, where  $\kappa_v$  is as unrealistically large as  $10^{-3} \text{ m}^2 \text{ s}^{-1}$ , and their residual is still balanced by a nonnegligible horizontal eddy density transport. In the cases using large values of interior  $\kappa_v$  (starting from the  $\kappa_v \times 10$  case), the near-bottom  $\sigma_2$  budget shows a dominant balance between horizontal mean flow advection and explicit vertical diffusion. A similar balance has been discussed by Mashayek et al. (2015) where it is related to an abyssal layer whose isopycnals intersect the flat bottom nearly vertically.

In summary, we have so far shown that the isopycnal slopes in the Southern Ocean channel do respond to changes in vertical diffusivity in the interior, even though the surface wind forcing is held constant in all the simulations. This is consistent with the results, in the limit of strong vertical mixing, of Nikurashin and Vallis (2011, 2012), who did not address the issue of the near-exponential vertical structure of middepth ocean stratification that is our focus. Thus, SO wind and eddies cannot set these slopes independently of interior vertical mixing when this vertical mixing is strong. The profile of  $\sigma_2$  agrees well with its exponential fit even when the interior  $\kappa_v$  is very weak. However, the quality of the exponential fit of  $\partial_z \sigma_2$  is not as good as observed for weak vertical mixing and improves as the interior  $\kappa_v$  is increased.

#### b. Southern Ocean response

We have pointed out that the isopycnal slopes in the Southern Ocean channel become steeper as the interior  $\kappa_v$  is increased. Steeper isopycnal slopes imply stronger baroclinic instability and therefore more vigorous eddy activity in the

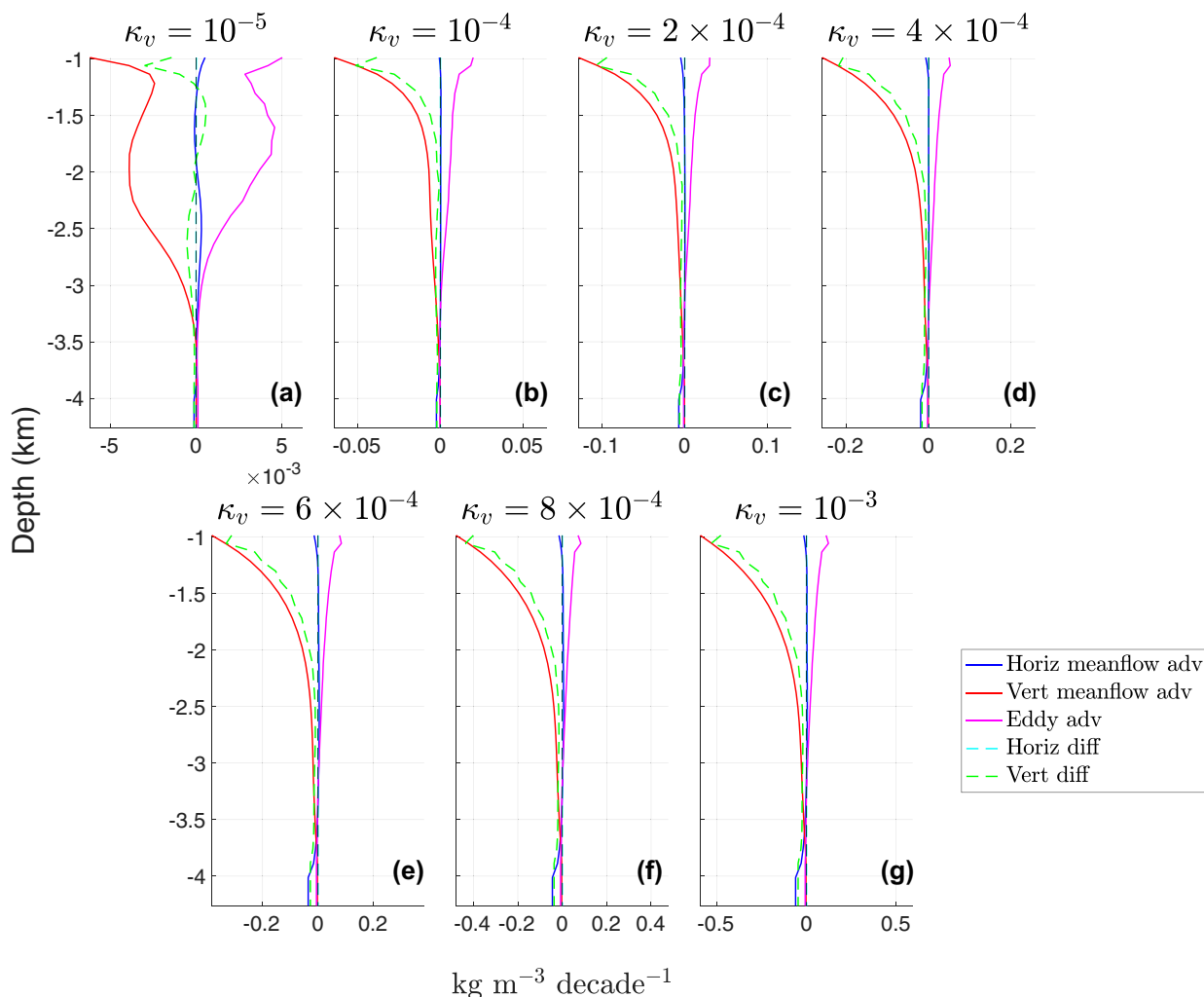


FIG. 6. Vertical profiles for different terms in the  $\sigma_2$  budget (horizontal mean-flow advection + vertical mean-flow advection + eddy advection = horizontal diffusion + vertical diffusion). Solid lines are for terms on the left-hand side and dashed lines are for terms on the right-hand side. The vertical profiles are averaged from  $30^\circ\text{S}$  to  $30^\circ\text{N}$ , in regions at least three degrees from the western and the eastern boundaries. Solid blue line: horizontal mean flow advection; solid red line: vertical mean flow advection; solid cyan line: eddy advection; dashed black line: explicit horizontal diffusion; dashed green line: explicit vertical diffusion. (a) Control, (b)  $\kappa_v \times 10$ , (c)  $\kappa_v \times 20$ , (d)  $\kappa_v \times 40$ , (e)  $\kappa_v \times 60$ , (f)  $\kappa_v \times 80$ , and (g)  $\kappa_v \times 100$ .

channel. Eddy kinetic energy [EKE;  $\sqrt{(u^2 + v^2)/2}$ ] averaged in different parts of the domain is shown in Fig. 7a. It is clear that eddy kinetic energy in the channel is increasing with the interior  $\kappa_v$ , with a smaller increase in the interior basin (away from the SO) as well. A similar steepening of SO isopycnals was explained by Munday et al. (2013) to be a result of deeper interior isopycnals due to stronger downward heat diffusion there. Munday et al. (2013) increased  $\kappa_v$  uniformly (including in the SO channel) and explored a smaller range of  $\kappa_v$ , but their explanation holds here as well, and this issue is briefly further explored next. The increase in eddy kinetic energy is consistent with changes in the Eady growth rate (Fig. 7b) and with an eddy energy production by enhanced baroclinic instability (appendix A, Fig. S11), as discussed in the supplemental material.

As a final approach to analyzing the change to the SO eddies, we consider a Gent and McWilliams (1990) type parameterization of the eddy-driven meridional circulation, where the eddy-driven meridional streamfunction  $\psi^*$  is assumed related to the isopycnal slopes  $S_\rho$  as  $\psi^* = \kappa_{GM} S_\rho$  (appendix C). We calculate the eddy streamfunction and slopes and diagnose  $\kappa_{GM}$ . As the SO eddies get stronger with interior  $\kappa_v$ , the diagnosed  $\kappa_{GM}$  linearly increases, with the averaged isopycnal slope in the SO channel (Fig. S4), consistent with Visbeck et al. (1997). This implies that it may not be appropriate to assume a constant  $\kappa_{GM}$  in simple box models for the middepth stratification and the related overturning circulation, and also in low-resolution ocean simulations. Note that the calculation of  $\kappa_{GM}$  in appendix C does not eliminate the effect of standing meanders and therefore is not necessarily equivalent to a

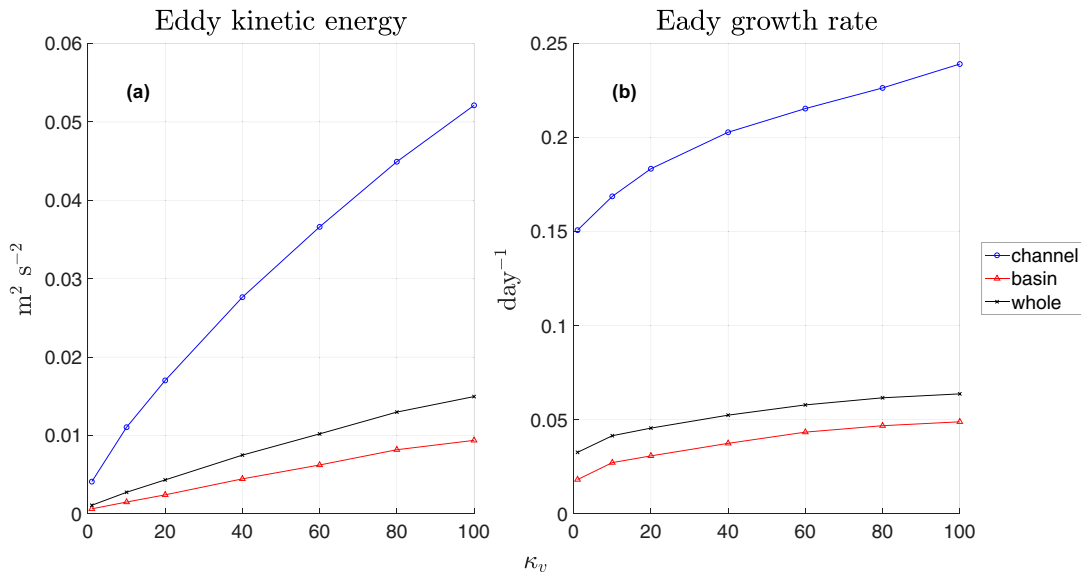


FIG. 7. (a) Averaged eddy kinetic energy  $[\sqrt{(u'^2 + v'^2)}/2]$ , as a function of interior  $\kappa_v$  ( $\times 10^5$ ). (b) Averaged Eady growth rate  $(0.31f|\partial_z \mathbf{u}_H|/N)$ . Blue line with circles: in the channel; red line with triangles: in the basin; black line with crosses: in the whole basin.

calculation of the same quantity from tracer fluxes and gradients, or based on mixing length theories (Ferrari and Nikurashin 2010).

To summarize this subsection, we find that while Southern Ocean eddies get stronger with the interior  $\kappa_v$ , the isopycnal flattening by eddies is not sufficiently efficient to prevent isopycnal slopes from changing. The SO isopycnal slopes are therefore still affected by the interior diapycnal mixing, and so is the middepth interior stratification.

#### 4. Discussion

Consider the two possible mechanisms by which SO eddies can affect the isopycnal slopes there, as discussed in section 3b. The wind-induced overturning steepens isopycnal surfaces, which gives rise to baroclinic instability and eddies. These eddies act to flatten the isopycnal surfaces by drawing APE from the slopes, and this competition between wind forcing and eddies will determine the slope of the isopycnal surfaces. Representing eddies by the thickness diffusivity  $\kappa_{GM}$  and assuming it is constant, the isopycnal slope  $S_\rho$  converges to  $S_\rho = (\psi_{res} + \tau^x/f)/\kappa_{GM}$  (Marshall and Radko 2003). When the wind forcing exactly balances the effect of the eddies, the SO residual deep circulation  $\psi_{res}$  vanishes, leading to a condition on the slope magnitudes,  $S_\rho = \tau^x/(f\kappa_{GM})$  (Marshall and Radko 2003). Previous work has shown that the SO residual deep circulation tends to vanish for weak interior diapycnal mixing, and that, remarkably, the interior stratification (as quantified by  $\partial_z \sigma_2$ , for example) does not vanish at this limit, in contradiction with the Munk picture (Wolfe and Cessi 2010; Nikurashin and Vallis 2011). However, we show that while the interior stratification indeed does not vanish at the limit of small diapycnal mixing, it is very far from the observed

near-exponential shape in that limit. We also calculated the residual circulation for our different interior diffusivity runs and found that the strength of the deep cell in the SO varies and does not necessarily vanish [consistent with the prediction of Marshall and Radko (2003)] for values of the interior diapycnal mixing that lead to near-exponential middepth stratification.

An alternative way to examine the role of eddies in setting SO isopycnal slopes involves the concept of marginal criticality. In this picture, as the external processes generating the slopes (SO winds) get stronger, the SO isopycnal slopes initially steepen. The resulting stronger baroclinic instability strengthens the eddies, draws APE from the slopes and acts to flatten them until the slopes are back to marginal criticality (Stone 1978; Jansen and Ferrari 2012, 2013a,b). At this point the processes generating the slopes exactly balance the effect of the eddies. This suggests that the slope and eddies are at saturation and do not respond to increased external SO wind forcing. However, we found that as we vary the interior diffusivity, the Southern Ocean eddies are unable to maintain a mean state of marginal criticality. This is consistent with the ratio between the Rhines scale and the deformation radius (Jansen and Ferrari 2013a) being significantly larger than one in our simulations. The inconsistency with marginal criticality means that the isopycnal slopes, and therefore also the middepth interior stratification, are not determined by the SO wind-eddy dynamics alone. Instead, the slopes are determined by an interplay of both interior diffusion that adjusts the density profile in the interior and therefore also at the northern edge of the SO, and the eddy processes striving for marginal stability within the SO.

The above measure of criticality (Jansen and Ferrari 2012) does not take into account dissipation. A dissipation such as

vertical diffusivity ( $\kappa_v$ ) can, in principle, shift the wavelength corresponding to the threshold of instability (Pedlosky 1987) as well as the critical isopycnal slope. However, our experiments do not change the vertical diffusivity within the SO itself; this means that SO baroclinic instability is not affected by the changing vertical diffusivity and that we may be justified using an inviscid and adiabatic criticality measure. On the other hand, the fact that we only marginally resolve eddy motions in the Southern Ocean (resolution there is about 15 km, of the same order as the Rossby radius) can affect our quantitative results for the criticality of the isopycnal slopes.

We conclude that whether we consider eddy processes from the point of view of residual circulation or marginal criticality in the SO, in the parameter regime corresponding to an exponential middepth  $\partial_z \sigma_2$  profile, Southern Ocean isopycnal slopes are not determined only by eddies and winds. Instead, SO eddies, and therefore also the isopycnal slopes there, respond to changes in interior stratification as well. This means that the communication between the Southern Ocean and the closed basin is not one-way (SO wind and eddies affecting middepth interior stratification) and that changes in the interior stratification also trigger responses in the Southern Ocean. This two-way interaction is complex, yet the principle governing the final outcome is simple (Tziperman 1986): the total mass flux across an isopycnal needs to vanish at a steady state. For isopycnals that outcrop in the SO, the near-surface Ekman transport is from dense water to light water. Eddy fluxes tend to be adiabatic (along-isopycnal), yet near the surface the vertical eddy buoyancy flux vanishes, allowing eddies to contribute to cross-isopycnal fluxes (Marshall and Radko 2003). Together, these water mass transformations by near-surface processes in outcropping areas of deep water need to be balanced by vertical mixing in the ocean interior. Because the magnitude of interior mixing depends on the ocean stratification (i.e., on vertical derivatives of the interior density), this leads to a global constraint on the interior middepth stratification.

One may think about the middepth stratification as being determined by a combination of slow and fast time scales: the SO eddies adjust the isopycnal slopes on short time scales, and the interior diffusivity responds on a time scale of hundreds of years, until the two are in equilibrium with each other. This is somewhat similar to the stratification of the upper ventilated thermocline being determined by potential vorticity conservation with the stratification specified on the eastern boundary (Luyten et al. 1983), with this eastern boundary stratification determined on a slower time scale by diapycnal mixing based on the above principle (Tziperman 1986).

## 5. Conclusions

Observations show that both the mean density profiles and the mean  $N^2$  profiles are very nearly exponential over large regions of the middepth (1–3 km) World Ocean (e.g., Miller et al. 2020; Figs. S7–S9). A vertical advective–diffusive balance was proposed to explain the near-exponential profile of temperature in the Pacific Ocean by Munk (1966). This explanation assumed that deep water formation returns to the surface via upwelling driven by diapycnal mixing in the ocean

interior. However, the vertical diffusivity in the middepth ocean required in this scenario is an order of magnitude larger than the values revealed by tracer release experiments (Ledwell et al. 1993; Polzin et al. 1997). An alternative mechanism leading to a nonvanishing middepth ocean stratification involves the SO wind steepening the isopycnals in the SO and eddies flattening them. The resulting SO isopycnal slopes map the SO surface density to a vertical interior profile (Wolfe and Cessi 2010; Nikurashin and Vallis 2011, 2012). While SO eddies have been shown to lead in this way to a nonvanishing middepth stratification at the limit of vanishing diapycnal mixing, the resulting stratification (buoyancy frequency profile or  $\partial_z \sigma_2$ ) is not exponential even if the density itself is nearly exponential (Miller et al. 2020). The observed near-exponential profile of the middepth stratification is thus unexplained, and this is the focus of the present work. We discussed in the introduction—and analyzed in the results section—two ways in which one can understand the effect of SO eddies on these slopes, involving either the residual circulation or marginal criticality. The results of this paper resonate with those of Miller et al. (2020) that the exponential vertical structure of the middepth ocean stratification requires a strong enough interior vertical mixing. The novel aspects of this paper compared to Miller et al. (2020) include 1) that we use eddy-permitting simulations, allowing us to directly study the interaction between SO eddy dynamics and the interior and 2) that we focus on the interaction between SO and interior, while Miller et al. (2020) focused on the equivalent effects on the mean middepth stratification of boundary-intensified vertical mixing and larger interior vertical mixing (see also Munk and Wunsch 1998).

We used idealized configurations of the MITgcm, at an eddy-permitting resolution, to examine how SO eddies can interact with diabatic mixing in the ocean interior (i.e., north of the SO), to determine the interior middepth exponential profiles of  $\sigma_2$  and  $\partial_z \sigma_2$ . We did so by varying vertical diffusivity only in the basin interior north of the SO. We found that both SO isopycnal slopes and the interior stratification respond to interior vertical diffusivity even as the wind forcing and Southern Ocean vertical mixing are unchanged. As the SO isopycnal slopes change in our experiments, so does their criticality and the SO residual circulation. This suggests that SO eddies and winds are not likely to determine the SO isopycnal slopes independently of processes north of the SO, diapycnal mixing in particular. This is consistent with previous work that found that the SO residual circulation depends on the interior diapycnal diffusivity, which, however, only addressed the mechanism for the existence of middepth stratification rather than its near-exponential vertical structure (Marshall and Radko 2003; Nikurashin and Vallis 2011, 2012).

We find that as interior vertical mixing increases, the SO slopes steepen and the vertical profile of  $\partial_z \sigma_2$  becomes more exponential. While previous work successfully showed that the middepth interior stratification does not vanish as the interior vertical diffusion goes to zero (Wolfe and Cessi 2010), we emphasize here that the  $\partial_z \sigma_2$  profile becomes exponential as observed only for larger interior diffusivity values. These

large diffusivity cases considered here are in apparent contradiction with the abovementioned tracer release experiments but may be physically realized in the ocean by a scenario of high vertical diffusion near ocean margins only (Munk and Wunsch 1998; Miller et al. 2020).

There are several caveats to note. First, the model configuration used here is an idealization of the Atlantic Ocean (our surface buoyancy boundary conditions induce deep water formation at both the northern high latitudes and near the southern boundary), but the vertical advective–diffusive balance is expected to work better in the Pacific Ocean where the upper cell of the overturning circulation does not exist (e.g., Nadeau and Jansen 2020; Baker et al. 2021). Second, we only use a single-basin configuration, and the communication between an Atlantic-type basin (with deep water formation) and a Pacific-type basin (without deep water formation) is missing. Third, it is, of course, artificial to only change the value of vertical mixing in the interior, although this strategy was adopted here to successfully answer a very specific question rather than used for a simulation of a realistic parameter regime. Some of the vertical diffusivity values we used in this study, especially those leading to exponential  $\partial_z \sigma_2$  profiles, are also unrealistically large. However, as explained, these values may be thought of as representing globally averaged values due to enhanced boundary mixing (Munk and Wunsch 1998; Miller et al. 2020). Miller et al. (2020) showed explicitly, in fact, that a Munk-like balance can hold in narrow boundary regions near ocean margins, with much larger vertical mixing and vertical velocity there. This results in a Munk-like balance and stratification that is then advected toward the ocean interior where the diffusivity may be small, consistent with tracer release experiments and with a similar suggestion made by Munk and Wunsch (1998). The need to use a large value of vertical diffusivity may also be partially due to our choice of a narrow basin (due to computational resources constraints), which has been shown to result in relatively weak and shallow overturning circulation (Nadeau and Jansen 2020).

*Acknowledgments.* XY and ET are supported by a Joint National Science Foundation/NERC, NSF Climate Dynamics Program Grant AGS-1924538. We would like to acknowledge high-performance computing support from Cheyenne provided by NCAR’s Computational and Information Systems Laboratory, sponsored by the National Science Foundation. ET thanks the Weizmann Institute for its hospitality during parts of this work.

*Data availability statement.* The MITgcm 3D ocean model used for this work is a community-developed model available for download from [http://mitgcm.org/public/source\\_code.html](http://mitgcm.org/public/source_code.html). All data, MITgcm modifications, vorticity model codes, and analysis scripts used in this work are archived in the “Open Science Framework,” which is a public, community-supported repository, at <https://osf.io/agtmq/>. These codes are publicly available, with no restrictions. The authors declare no conflict of interests.

## APPENDIX A

### Eddy Kinetic Energy Budget

Following Zhai and Marshall (2013), the budget of eddy kinetic energy [ $\overline{E} \equiv (u'^2 + v'^2)/2$ ] can be written as

$$\frac{\partial \overline{E}}{\partial t} + \nabla \cdot \left( \overline{\mathbf{v}E} + \frac{\overline{p'\mathbf{v}'}}{\rho_0} \right) - \overline{\mathbf{u}' \cdot \mathbf{F}'} + \overline{\mathbf{u}' \cdot (\mathbf{v}' \cdot \nabla \mathbf{u})} = - \frac{\overline{\rho' w' g}}{\rho_0}. \quad (\text{A1})$$

In this equation,  $\overline{(\cdot)}$  stands for the time mean;  $(\cdot)'$  stands for the deviation from the time mean;  $\mathbf{u} \equiv (u, v)$  is the horizontal velocity vector;  $\mathbf{v} \equiv (u, v, w)$  is the 3D velocity vector;  $\rho$  is density;  $\rho_0$  is a reference density;  $g$  is gravitational acceleration;  $p$  is pressure; and  $\mathbf{F}$  is the friction term.

Following Zhai and Marshall (2013), the  $\nabla \cdot \overline{p'\mathbf{v}'}/\rho_0$  terms are the eddy energy flux, and  $-\overline{w'\rho'g}/\rho_0$  is the eddy energy associated with baroclinic instability.

## APPENDIX B

### Length Scales in the Southern Ocean Channel and Criticality

Following Chelton et al. (1998), we define the deformation radius as

$$L_d = \frac{1}{\pi} \int_{\text{bot}}^{\text{top}} \frac{N dZ}{f}, \quad (\text{B1})$$

in which  $f = 2\omega \sin(\theta)$  is the Coriolis parameter, and  $N^2 = -g \partial_z \rho / \rho_0$  is the buoyancy frequency.

We define the Rhines scale at which the upper-scale energy cascade should halt as

$$L_b = 2\pi \frac{\text{EKE}_t^{1/4}}{\beta^{1/2}}, \quad (\text{B2})$$

in which  $\text{EKE}_t$  is the barotropic eddy kinetic energy, and  $\beta = 2\omega \cos(\theta)/R$  is the meridional gradient of the Coriolis parameter. The criticality parameter is further defined as the ratio between  $R_b$  and  $R_d$ , averaged in the SO channel.

## APPENDIX C

### Residual Overturning Circulation and Horizontal Eddy Diffusivity

The residual overturning circulation as a function of latitude  $y$  and buoyancy  $b_0$  is calculated following Wolfe and Cessi (2011) as

$$\psi_{\text{res}}(y, b_0) = -\frac{1}{T} \int_0^T \int_0^{L_x} \int_{\text{bot}}^{\text{top}} v(x, y, z, t) \mathcal{R}[b(x, y, z, t) - b_0] dz dx dt, \quad (\text{C1})$$

in which  $T$  is an averaging time period,  $L_x$  is the zonal extent of the basin,  $v$  is the meridional velocity, and  $\mathcal{R}$  is the

Heaviside function. The zonal- and time-averaged height of a surface of constant buoyancy  $b_0$  is calculated as

$$Z(y, b_0) = \frac{1}{T} \int_0^T \int_0^{L_x} \int_{\text{bot}}^{\text{top}} \mathcal{H}[b(x, y, z, t) - b_0] dz dx dt. \quad (\text{C2})$$

The residual overturning circulation can then be interpolated to depth coordinate using the  $Z$  field (Fig. S5) and denoted  $\tilde{\psi}_{\text{res}}(y, z)$ .

Following Marshall and Radko (2003), the residual meridional velocity  $\tilde{v}_{\text{res}} \equiv -\partial_z \tilde{\psi}_{\text{res}}$  can be decomposed into the Eulerian component  $\bar{v} \equiv -\partial_z \bar{\psi}$  and an eddy-induced component  $v_{\text{eddy}} \equiv \tilde{v}_{\text{res}} - \bar{v}$ , which may be written in terms of a corresponding streamfunction as  $v_{\text{eddy}} = -\partial_z \psi_{\text{eddy}}$ . The residual momentum equation is now

$$f \frac{\partial \tilde{\psi}_{\text{res}}}{\partial z} = \bar{F} + f \frac{\partial \psi_{\text{eddy}}}{\partial z} = \frac{\partial \bar{\tau}}{\partial z} + f \frac{\partial \psi_{\text{eddy}}}{\partial z}, \quad (\text{C3})$$

in which  $\bar{F}$  represents momentum flux divergence. Neglecting the horizontal divergence terms (Gille 2003), the  $\bar{F}$  term is further rewritten in the last equality above as  $\bar{F} = \partial_z \bar{\tau}$ .

Vertically integrating Eq. (C3), assuming that the residual and eddy-driven overturning cells vanish at the surface, and letting  $\tau(y, z = 0)$  be equal to the wind stress, the residual circulation in the channel can be decomposed into a wind-induced part and an eddy-induced part

$$\begin{aligned} \tilde{\psi}_{\text{res}}(y, z) &= -\frac{\tau^{\text{wind}}(y)}{\rho_0 f} + \psi_{\text{eddy}}(y, z) \\ &= -\frac{\tau^{\text{wind}}(y)}{\rho_0 f} + \kappa_{\text{GM}}(y, z) S_\rho(y, z) \\ &= -\frac{\tau^{\text{wind}}(y)}{\rho_0 f} - \kappa_{\text{GM}}(y, z) \frac{\partial_y \sigma_2}{\partial_z \sigma_2}, \end{aligned} \quad (\text{C4})$$

with a Gent–McWilliams-type parameterization assumed in the last equality. The parameter  $\kappa_{\text{GM}}$  calculated following Eq. (C4) is shown in Fig. S4.

## REFERENCES

- Baker, J. A., A. J. Watson, and G. K. Vallis, 2021: Meridional overturning circulation in a multibasin model. Part II: Sensitivity to diffusivity and wind in warm and cool climates. *J. Phys. Oceanogr.*, **51**, 1813–1828, <https://doi.org/10.1175/JPO-D-20-0121.1>.
- Chelton, D. B., R. A. DeSzoeke, M. G. Schlax, K. El Naggar, and N. Siwertz, 1998: Geographical variability of the first baroclinic Rossby radius of deformation. *J. Phys. Oceanogr.*, **28**, 433–460, [https://doi.org/10.1175/1520-0485\(1998\)028<0433:GVOTFB>2.0.CO;2](https://doi.org/10.1175/1520-0485(1998)028<0433:GVOTFB>2.0.CO;2).
- Ferrari, R., and M. Nikurashin, 2010: Suppression of eddy diffusivity across jets in the Southern Ocean. *J. Phys. Oceanogr.*, **40**, 1501–1519, <https://doi.org/10.1175/2010JPO4278.1>.
- , A. Mashayek, T. J. McDougall, M. Nikurashin, and J.-M. Campin, 2016: Turning ocean mixing upside down. *J. Phys. Oceanogr.*, **46**, 2239–2261, <https://doi.org/10.1175/JPO-D-15-0244.1>.
- Gent, P. R., and J. C. McWilliams, 1990: Isopycnal mixing in ocean circulation models. *J. Phys. Oceanogr.*, **20**, 150–155, [https://doi.org/10.1175/1520-0485\(1990\)020<0150:IMIOCM>2.0.CO;2](https://doi.org/10.1175/1520-0485(1990)020<0150:IMIOCM>2.0.CO;2).
- Gille, S. T., 2003: Float observations of the Southern Ocean. Part II: Eddy fluxes. *J. Phys. Oceanogr.*, **33**, 1182–1196, [https://doi.org/10.1175/1520-0485\(2003\)033<1182:FOOTSO>2.0.CO;2](https://doi.org/10.1175/1520-0485(2003)033<1182:FOOTSO>2.0.CO;2).
- Gnanadesikan, A., 1999: A simple predictive model for the structure of the oceanic pycnocline. *Science*, **283**, 2077–2079, <https://doi.org/10.1126/science.283.5410.2077>.
- Gouretski, V., and K. P. Koltermann, 2004: WOCE global hydrographic climatology. *Berichte des BSH 35/2004*, 52 pp., [https://rda.ucar.edu/datasets/ds285.4/docs/bsh35\\_re.pdf](https://rda.ucar.edu/datasets/ds285.4/docs/bsh35_re.pdf).
- Jackett, D. R., and T. J. McDougall, 1995: Minimal adjustment of hydrographic profiles to achieve static stability. *J. Atmos. Oceanic Technol.*, **12**, 381–389, [https://doi.org/10.1175/1520-0426\(1995\)012<0381:MAOHPT>2.0.CO;2](https://doi.org/10.1175/1520-0426(1995)012<0381:MAOHPT>2.0.CO;2).
- Jansen, M., and R. Ferrari, 2012: Macroturbulent equilibration in a thermally forced primitive equation system. *J. Atmos. Sci.*, **69**, 695–713, <https://doi.org/10.1175/JAS-D-11-041.1>.
- , and —, 2013a: Equilibration of an atmosphere by adiabatic eddy fluxes. *J. Atmos. Sci.*, **70**, 2948–2962, <https://doi.org/10.1175/JAS-D-13-013.1>.
- , and —, 2013b: The vertical structure of the eddy diffusivity and the equilibration of the extratropical atmosphere. *J. Atmos. Sci.*, **70**, 1456–1469, <https://doi.org/10.1175/JAS-D-12-086.1>.
- Large, W. G., J. McWilliams, and S. Doney, 1994: Oceanic vertical mixing: A review and a model with a nonlocal boundary layer parameterization. *Rev. Geophys.*, **32**, 363–403, <https://doi.org/10.1029/94RG01872>.
- Ledwell, J. R., A. J. Watson, and C. S. Law, 1993: Evidence for slow mixing across the pycnocline from an open-ocean tracer-release experiment. *Nature*, **364**, 701–703, <https://doi.org/10.1038/364701a0>.
- Luyten, J. R., J. Pedlosky, and H. Stommel, 1983: The ventilated thermocline. *J. Phys. Oceanogr.*, **13**, 292–309, [https://doi.org/10.1175/1520-0485\(1983\)013<0292:TVT>2.0.CO;2](https://doi.org/10.1175/1520-0485(1983)013<0292:TVT>2.0.CO;2).
- Marshall, J., and T. Radko, 2003: Residual-mean solutions for the Antarctic Circumpolar Current and its associated overturning circulation. *J. Phys. Oceanogr.*, **33**, 2341–2354, [https://doi.org/10.1175/1520-0485\(2003\)033<2341:RSFTAC>2.0.CO;2](https://doi.org/10.1175/1520-0485(2003)033<2341:RSFTAC>2.0.CO;2).
- , A. Adcroft, C. Hill, L. Perelman, and C. Heisey, 1997: Hydrostatic, quasi-hydrostatic and nonhydrostatic ocean modeling. *J. Geophys. Res.*, **102**, 5733–5752, <https://doi.org/10.1029/96JC02776>.
- Mashayek, A., R. Ferrari, M. Nikurashin, and W. Peltier, 2015: Influence of enhanced abyssal diapycnal mixing on stratification and the ocean overturning circulation. *J. Phys. Oceanogr.*, **45**, 2580–2597, <https://doi.org/10.1175/JPO-D-15-0039.1>.
- Miller, M. D., X. Yang, and E. Tziperman, 2020: Reconciling the observed mid-depth exponential ocean stratification with weak interior mixing and Southern Ocean dynamics via boundary-intensified mixing. *Eur. Phys. J. Plus*, **135**, 375, <https://doi.org/10.1140/epjp/s13360-020-00375-y>.
- Munday, D. R., L. Allison, H. Johnson, and D. Marshall, 2011: Remote forcing of the Antarctic circumpolar current by diapycnal mixing. *Geophys. Res. Lett.*, **38**, L08609, <https://doi.org/10.1029/2011GL046849>.
- , H. L. Johnson, and D. P. Marshall, 2013: Eddy saturation of equilibrated circumpolar currents. *J. Phys. Oceanogr.*, **43**, 507–532, <https://doi.org/10.1175/JPO-D-12-095.1>.

- Munk, W., and C. Wunsch, 1998: Abyssal recipes II: Energetics of tidal and wind mixing. *Deep-Sea Res. I*, **45**, 1977–2010, [https://doi.org/10.1016/S0967-0637\(98\)00070-3](https://doi.org/10.1016/S0967-0637(98)00070-3).
- Munk, W. H., 1966: Abyssal recipes. *Deep-Sea Res. Oceanogr. Abstr.*, **13**, 707–730, [https://doi.org/10.1016/0011-7471\(66\)90602-4](https://doi.org/10.1016/0011-7471(66)90602-4).
- Nadeau, L.-P., and M. F. Jansen, 2020: Overturning circulation pathways in a two-basin ocean model. *J. Phys. Oceanogr.*, **50**, 2105–2122, <https://doi.org/10.1175/JPO-D-20-0034.1>.
- Nikurashin, M., and G. Vallis, 2011: A theory of deep stratification and overturning circulation in the ocean. *J. Phys. Oceanogr.*, **41**, 485–502, <https://doi.org/10.1175/2010JPO4529.1>.
- , and —, 2012: A theory of the interhemispheric meridional overturning circulation and associated stratification. *J. Phys. Oceanogr.*, **42**, 1652–1667, <https://doi.org/10.1175/JPO-D-11-0189.1>.
- Pedlosky, J., 1987: *Geophysical Fluid Dynamics*. 2nd ed. Springer, 724 pp.
- Polzin, K., J. Toole, J. Ledwell, and R. Schmitt, 1997: Spatial variability of turbulent mixing in the abyssal ocean. *Science*, **276**, 93–96, <https://doi.org/10.1126/science.276.5309.93>.
- Samelson, R., 1998: Large-scale circulation with locally enhanced vertical mixing. *J. Phys. Oceanogr.*, **28**, 712–726, [https://doi.org/10.1175/1520-0485\(1998\)028<0712:LSCWLE>2.0.CO;2](https://doi.org/10.1175/1520-0485(1998)028<0712:LSCWLE>2.0.CO;2).
- Scott, J. R., and J. Marotzke, 2002: The location of diapycnal mixing and the meridional overturning circulation. *J. Phys. Oceanogr.*, **32**, 3578–3595, [https://doi.org/10.1175/1520-0485\(2002\)032<3578:TLODMA>2.0.CO;2](https://doi.org/10.1175/1520-0485(2002)032<3578:TLODMA>2.0.CO;2).
- Stone, P. H., 1978: Baroclinic adjustment. *J. Atmos. Sci.*, **35**, 561–571, [https://doi.org/10.1175/1520-0469\(1978\)035<0561:BA>2.0.CO;2](https://doi.org/10.1175/1520-0469(1978)035<0561:BA>2.0.CO;2).
- Tziperman, E., 1986: On the role of interior mixing and air–sea fluxes in determining the stratification and circulation of the oceans. *J. Phys. Oceanogr.*, **16**, 680–693, [https://doi.org/10.1175/1520-0485\(1986\)016<0680:OTROIM>2.0.CO;2](https://doi.org/10.1175/1520-0485(1986)016<0680:OTROIM>2.0.CO;2).
- Vallis, G. K., 2000: Large-scale circulation and production of stratification: Effects of wind, geometry, and diffusion. *J. Phys. Oceanogr.*, **30**, 933–954, [https://doi.org/10.1175/1520-0485\(2000\)030<0933:LSCAPO>2.0.CO;2](https://doi.org/10.1175/1520-0485(2000)030<0933:LSCAPO>2.0.CO;2).
- Visbeck, M., J. Marshall, T. Haine, and M. Spall, 1997: Specification of eddy transfer coefficients in coarse-resolution ocean circulation models. *J. Phys. Oceanogr.*, **27**, 381–402, [https://doi.org/10.1175/1520-0485\(1997\)027<0381:SOETCI>2.0.CO;2](https://doi.org/10.1175/1520-0485(1997)027<0381:SOETCI>2.0.CO;2).
- Wolfe, C. L., and P. Cessi, 2010: What sets the strength of the middepth stratification and overturning circulation in eddy ocean models? *J. Phys. Oceanogr.*, **40**, 1520–1538, <https://doi.org/10.1175/2010JPO4393.1>.
- , and —, 2011: The adiabatic pole-to-pole overturning circulation. *J. Phys. Oceanogr.*, **41**, 1795–1810, <https://doi.org/10.1175/2011JPO4570.1>.
- Wunsch, C., and R. Ferrari, 2004: Vertical mixing, energy and the general circulation of the oceans. *Annu. Rev. Fluid Mech.*, **36**, 281–314, <https://doi.org/10.1146/annurev.fluid.36.050802.122121>.
- Zhai, X., and D. P. Marshall, 2013: Vertical eddy energy fluxes in the North Atlantic subtropical and subpolar gyres. *J. Phys. Oceanogr.*, **43**, 95–103, <https://doi.org/10.1175/JPO-D-12-021.1>.